Journal of Power Sources 209 (2012) 209–219

Contents lists available at SciVerse ScienceDirect

Journal of Power Sources

journal homepage: www.elsevier.com/locate/jpowsour

High-performance $Gd_{0.2}Ce_{0.8}O_2$-impregnated $LaNi_{0.6}Fe_{0.4}O_{3-\delta}$ cathodes for intermediate temperature solid oxide fuel cell

Bo Huang*, Xin-jian Zhu, Yao Lv, Heng Liu

Institute of Fuel Cell, School of Mechanical Engineering, Shanghai Jiaotong University, 800 Dongchuan Road, Shanghai 200240, PR China

ARTICLE INFO

Article history:
Received 9 January 2012
Received in revised form 23 February 2012
Accepted 26 February 2012
Available online 5 March 2012

Keywords:
Cathode
High performance
Impregnation
Solid oxide fuel cell
Specific polarization resistance

ABSTRACT

High-performance $LaNi_{0.6}Fe_{0.4}O_{3-\delta}$ (LNF) cathode for intermediate temperature solid oxide fuel cell is fabricated by the ion impregnation of oxygen ion conducting Gd-doped ceria (GDC, $Gd_{0.2}Ce_{0.8}O_2$). The microstructure of the GDC-impregnated LNF cathode is characterized by the dispersion of nano-sized GDC particles in the LNF porous framework. The particle size of the impregnated GDC phase is in the range of 40–50 nm. Uniform distribution of the nano-sized ionic conducting GDC phase significantly enhances the cathode activities for the O_2 reduction reaction. In the case of the 21.3 wt.% GDC-impregnated LNF cathode, the specific polarization resistance (R_p) is 0.13 $\Omega\,cm^2$ at 750 °C, a reduction by 81.43% compared with that of the pure LNF cathode at the same temperature. The results indicate that GDC impregnation has significant electrocatalytic effect on the O_2 reduction reactions on the LNF cathodes. The improved performance of GDC-impregnated LNF cathode is attributed to the extended triple-phase boundary (TPB) and enhanced oxide ion conductivity.

1. Introduction

Reducing the operating temperature of solid oxide fuel cell (SOFC) down to 600–800 °C brings both dramatic economic and technical benefits. The cost of SOFC technology may be dramatically reduced since much less expensive materials can be used in cell construction and novel fabrication techniques can be applied to the stack and system integration. Further, the reduction in the operating temperature would greatly reduce the degradation of SOFC components, widen the materials selection, lessen the sealing problem, allow the use of metallic materials as the interconnects, and eventually accelerate the commercialization of SOFC technology. However, the performance of an SOFC system would decrease because of the low oxide ion conductivity of yttria-stabilized zirconia (YSZ), the high overpotential at the electrode and the increased polarization resistance of the electrodes, especially for the O_2 reduction reaction on the cathode side at lower operating temperature. The reduction of the thickness of the YSZ electrolyte [1], and the application of the $La(Sr)Ga(Mg)O_{3-\delta}$ (LSGM) [2–4] or gadolinium-doped ceria (GDC) [5] electrolyte material with higher ionic conductivity than YSZ, has all significantly reduced the ohmic loss from the electrolyte. Thus, the development of the cathode materials with high electrocatalytic activity becomes increasingly critical for intermediate temperature SOFC (IT-SOFC).

$La(Ni,Fe)O_3$ perovskite material has been developed as one of the most promising cathode materials in IT-SOFC operated at 600–800 °C. Of particular interest is $LaNi_{0.6}Fe_{0.4}O_3$ (LNF) which exhibits high electronic conductivity, a thermal expansion coefficient close to that of the zirconia electrolyte, high electrochemical activity for the oxygen reduction reaction, and resistance to cathode poisoning by chromia vapor from the metal separators [6–9]. However, the initial performance of the LNF cathode is not very high [8], and it gradually improves with cell operation time. More than a hundred hours is required for the cathode to reach a stable state at which point the LNF cathode exhibits very high levels of performance [8]. This gradual improvement in the performance of the LNF cathode are considered to be attributed to several causes including the sintering of the cathode or disappearance of the $La_2Zr_2O_7$ phase at the cathode electrolyte interface during the current loading process [10,11]. The sintering of the LNF cathode leads to an improvement in its electrical conductivity. The sintering at the interface between the LNF cathode and electrolyte influence the cathode properties such as interface resistance [12], because the bonds between the LNF cathode particles and the electrolyte are strengthened.

$La_2Zr_2O_7$ is formed by the reaction between the zirconia electrolyte and the LNF cathode [13] when the sintering temperature is high. The formation of the $La_2Zr_2O_7$ leads to cathode degradation because of the low electronic and ionic conductivity of $La_2Zr_2O_7$. The poor performance of the LNF cathode prior to the current loading is considered to be associated with the $La_2Zr_2O_7$ formation [10,11]. Some studies have suggested that the effect of

* Corresponding author. Tel.: +86 21 34206249; fax: +86 21 34206249.
E-mail address: huangbo2k@hotmail.com (B. Huang).

0378-7753/$ – see front matter.
doi:10.1016/j.jpowsour.2012.02.103

a $La_2Zr_2O_7$ layer can be reduced by applying current loading to the cell [8,10,11]. The change in the LNF cathode performance during the current loading process is associated with the presence of $La_2Zr_2O_7$ [14].

Sm or Gd doped cerium oxides (SDC, GDC) materials are suitable as the interlayer between a cathode and a zirconia electrolyte, since they hardly react with most of the cathode materials with a perovskite structure, and furthermore, improve the electrocatalytic activities of the cathode. Xia et al. [15] studied the LSM/GDC composite cathodes fabricated by the sol–gel process. The sol–gel derived composite cathodes showed very low electrode polarization resistance, 0.16 Ω cm^2 at 750 °C, lower than that obtained by the slurry coating technique [16]. Liu et al. [17,18] used combustion chemical vapor deposition (CCVD) process to fabricate functionally graded LSM/LSC/GDC electrodes and achieved electrode polarization resistance of 0.43 Ω cm^2 at 700 °C. The GDC layer can prevent contact between the LSM cathode and the zirconia electrolyte and thus prevent the formation of $La_2Zr_2O_7$. The high electrocatalytic activity of the LSM-based cathode fabricated by combustion CVD has been attributed to the functionally graded and nanostructured interface. This indicates that, through the proper composition optimization and materials engineering of the cathode structure, the electrocatalytic activity of the cathode can be furthermore improved. The problem with using cerium oxide for the interlayer is its low sinterability. If the cerium oxide layer is prepared by a conventional method, such as screen-printing and sintering with a cathode (at 1000–1200 °C), the mechanical strength and adhesiveness are poor. If the layer is sintered with a zirconia electrolyte (at 1300–1400 °C), the cerium atoms penetrate the thin (10 μm thick) electrolyte [19] in the case of anode-supported cells. This will result in a lower ionic transport number for the zirconia electrolyte [20] and the increase in the ohmic resistance at the interface of SASZ and SDC interlayer.

Ion impregnation has been shown to be a very effective method to introduce nanosized electrocatalytic phases into the porous electrode structure. The technique involves depositing nanoparticles into a pre-sintered backbone. The sintering of backbone is performed at high temperature, which ensures good bonding between the electrode backbone and the electrolyte, good connection between the particles to achieve high effective conduction of electron or oxygen ion, and the structural stability of the cathode. The firing process for the deposition of nanoparticles and the formation of the desired phase can be conducted at temperature much lower than that needed for the traditional ceramic fabrication process. The low temperature fabrication has many advantages. Since the firing temperature is low, nanoscale characteristics of particles can be preserved which is beneficial to achieving high catalytic activity and large TPB length. Study shows that the TPB length in a cathode prepared by impregnation is much larger than that of the composite cathode prepared by the traditional ceramic mixing process [21]. In addition, the reaction between the cathodes and YSZ can be avoided as the firing temperature is low, making it possible to use materials with high electrochemical performance as cathodes for SOFC with YSZ electrolytes. The impregnation may also alleviate the thermal expansion mismatch problems. In a cathode fabricated by the impregnation process, the coefficient of thermal expansion (CTE) is dominated by the backbone materials, and impregnation the CTE mismatched materials has little effect on the CTE of the electrode. The performance of conventional LSM cathode can be significantly improved by the ion impregnation of mixed conducting oxides such as Gd-doped CeO_2 (GDC) [22–24]. Results show that, after the impregnation of 5.8 mg cm^{-2} GDC in the porous LSM cathode, the electrode polarization resistance is drastically reduced to 0.21 Ω cm^2 at 700 °C, which is 56 times smaller than that of the pure LSM cathode at the same temperature. In this paper, the fabrication and cathode behavior of the $Gd_{0.2}Ce_{0.8}O_2$ (GDC)-impregnated LNF cathode have been investigated. The results indicate that the impregnation of GDC phase substantially improves the performance of the LNF cathodes associated with the O_2 reduction reaction.

2. Experimental

2.1. Preparation and characterization of the $LaNi_{0.6}Fe_{0.4}O_{3-\delta}$ powder

The composition of LNF cathode was chosen as $LaNi_{0.6}Fe_{0.4}O_{3-\delta}$ [25]. $LaNi_{0.6}Fe_{0.4}O_{3-\delta}$ (LNF) cathode material was prepared using a combustion synthesis technique. Stoichiometric amounts of lanthanum nitrate ($La(NO_3)_3{\cdot}6H_2O$), nickel nitrate $Ni(NO_3)_2{\cdot}H_2O$ and ferric nitrate $Fe(NO_3)_3{\cdot}9H_2O$ were dissolved in distilled water with constant stirring. Then, a stoichiometric amount of citric acid ($C_6H_8O_7{\cdot}H_2O$), which is a chelating agent and fuel, was also dissolved in this solution. The stoichiometric ratio of citric acid to nitrates was calculated according to Jain et al. [26]. The solution pH was maintained between 7 and 8 with the addition of concentrated ammonia solution. A gel was formed with continuous stirring and mild heating (∼120 °C). The gel was dried at room temperature for over 12 h and then fired at 300 °C for 30 min. The resulting powders were ground in an agate mortar and fired at 600 °C for 2 h in air to obtain the powders of final composition ($LaNi_{0.6}Fe_{0.4}O_{3-\delta}$). X-ray diffraction (XRD) patterns were collected with a Philips X'Pert Pro diffractometer equipped with a primary monochromator (Cu Kα radiation) and a Philips X'Celerator detector for the structural characterization of the LNF powder. The scans were performed in the 2θ range 10–90° at the scanning speed of 4° min^{-1}. Further XRD studies were also carried out to investigate the chemical compatibility of LNF with ScSZ material. Powder mixture of LNF with ScSZ, in a 1:1 (wt.%) ratio, were ground in an agate mortar and fired at 1100 °C for 5 h. Field emission scanning electron microscope (FE-SEM) images of the interface layer LNF/ScSZ before and after the EIS measurement were analyzed using a microscope (FE-SEM, PHILIPS 515, Holland) equipped with an X-ray analyzer for energy-dispersive X-ray spectroscopy (EDS).

Simultaneous thermogravimetric-differential thermal analysis (TGA/DTA, Netzsch STA 409) were carried out in static air at heating/cooling rate of 10 °C min^{-1}, to determine the stoichiometry of the nitrates and to estimate the optimal crystallization temperature of the LNF precursor powders.

2.2. Preparation of the GDC-impregnated LNF cathode

ScSZ (scandia stabilized zirconia, $Sc_{0.1}Zr_{0.9}O_{1.95}$, 99.99% pure, Daiichi Kigenso, Japan) pellet with the diameter of 20 mm and the thickness of about 200 μm was used as the electrolyte. Electrolyte-supported symmetric cell for impedance testing was fabricated by screen printing method. The slurry of the LNF cathode powder, which was ground and mixed with isopropyl alcohol, was screen-printed onto both sides of the ScSZ electrolyte pellet. Then the symmetric cells were sintered at 1000, 1050, 1100 and 1150 °C for 2 h under stagnant air, respectively. After being sintered, the resulting LNF cathode areas are 1 cm^2. The LNF cathode is a square in shape. The side length of the square is 1 cm.

$Gd_{0.2}Ce_{0.8}O_2$ (GDC) precursor gel was prepared as follows. Initially, stoichiometric amounts of gadolinium nitrate ($Gd(NO_3)_3{\cdot}6H_2O$) and cerium nitrate ($Ce(NO_3)_3{\cdot}6H_2O$) were dissolved in distilled water with constant stirring. Then, a stoichiometric amount of citric acid ($C_6H_8O_7{\cdot}H_2O$), which is a chelating agent and fuel, was also dissolved in this solution. The stoichiometric ratio of citric acid to nitrates was calculated according to Jain et al. [26]. The Ce^{3+} concentration in the transparent solution

was 0.4 mol dm^{-3}. The solution pH was maintained between 7 and 8. The LNF cathode layers of electrolyte-supported symmetric cell sintered at 1050 °C were completely dipped in the above solution and evacuated using a vacuum pump set to an absolute pressure of 200 mbar for 10 min so that the solution filled the pores of the LNF cathode layer. Then it was dried at 75 °C, followed by calcination at 600 °C for 2 h to decompose $Gd_{0.2}Ce_{0.8}(NO_3)_x$ nitrate solution, forming $Gd_{0.2}Ce_{0.8}O_2$ oxide phase. This procedure was repeated several times to have a uniform and sufficient coating. The impregnated $Gd_{0.2}Ce_{0.8}O_2$ loading in the LNF cathode was estimated from the weight change of the LNF cathode coating before and after the impregnation treatment.

2.3. Measurement of the GDC-impregnated LNF cathode polarization

The polarization resistance of the GDC-impregnated LNF cathode was measured in the two-electrode symmetric cell configuration under air [27]. Pt mesh was attached to the electrode surfaces using Pt paste as the current collector. The electrochemical activities of the GDC-impregnated LNF cathodes were characterized by the electrochemical impedance spectroscopy (EIS), using a Solartron 1260 frequency response analyzer at open circuit. The applied frequency was in the range of 0.01 Hz to 100 kHz at five points per frequency decade with the signal amplitude of 20 mV. The EIS measurement was carried out in the temperature range of 600–850 °C in steps of 50 °C in the air. To stabilize the cathode behavior, LNF cathodes were polarized at 750 °C with a constant current density of 50 mA cm^{-2} for 2 h before the electrochemical testing. The specific ohmic resistance (R_Ω) was estimated from the high frequency intercept of the impedance curves and the specific polarization resistance (R_p) was directly measured from the differences between the low and high frequency intercepts on the impedance curves. Field emission scanning electron microscope (FE-SEM) images of the interface layer GDC-impregnated LNF/ScSZ before and after the EIS measurement were analyzed using a microscope (FE-SEM, PHILIPS 515, Holland) equipped with an X-ray analyzer for energy-dispersive X-ray spectroscopy (EDS). The porosity of the GDC-impregnated LNF cathode coating was estimated from the SEM images of the cross section of the cathode samples [28]. Five SEM images were usually taken from the different cross-section areas of the specimen and the pores were defined as black area in the binary images in a computer program [28]. From the porosity difference between the LNF cathodes with and without GDC impregnation, the volume percentage of the impregnated GDC phase in the LNF cathode was obtained.

3. Results and discussion

3.1. Characterization of the LNF powder

Fig. 1 shows the TGA–DTA curves of the LNF perovskite gel precursor dried at 120 °C. The percentage weight loss from room temperature to 1250 °C was 45.10 wt.%. It could be seen from the TGA curve that the mass of the gel decreased sharply in the temperature range of 150–300 °C, which was caused mainly by the redox reaction between the citric acid and metal nitrates. The DTA curve of the gel confirmed the result of TGA analysis perfectly. As is shown in the DTA curve, one sharp exothermic peak appeared in the temperature range of 150–300 °C, which can be attributed to the exothermic redox reaction between the fuel and nitrates. The weight remained constant above 450 °C.

Fig. 2 shows the X-ray diffraction (XRD) pattern of the combustion-synthesized LNF powder calcined at 600 °C for 2 h. The thermal treatment at 600 °C left only the LNF phase detectable as a

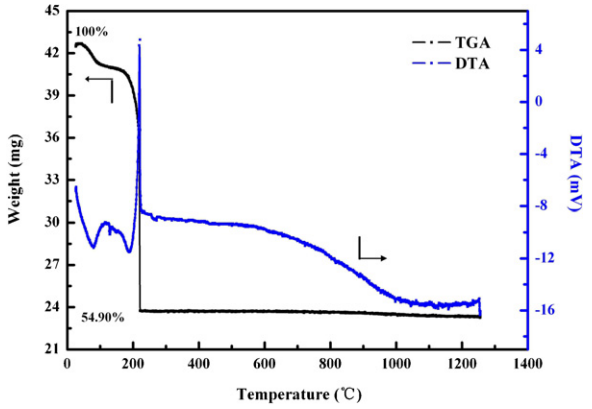

Fig. 1. TGA/DTA curves of the $LaNi_{0.6}Fe_{0.4}O_{3-\delta}$ perovskite gel precursor dried at 120 °C.

purity. The patterns are identical to the LNF powder obtained by a solid-state reaction method at 950 °C [25], indicating the formation of the perovskite phase of the LNF powder. Giving the combined results of TGA–DTA and XRD analyses, showing that the powder calcined at 600 °C was made nearly entirely of LNF single-phase.

3.2. AC impedance measurement

The typical impedance spectroscopies for the LNF cathode sintered at different temperatures measured at 650 °C (a), 700 °C (b), 750 °C (c), 800 °C (d) and 850 °C (e) in the air are shown in Fig. 3(a)–(e). As it can be seen from the corresponding Nyquist plots, the spectra are composed of one semicircle, which is associated with oxygen reduction at the LNF/ScSZ interfaces. The spectra were analyzed by considering an $R_p - Q$ parallel circuit with a series connection of R_Ω (R_p is the specific polarization resistance, Q is the constant phase element (CPE) and R_Ω indicates the specific ohmic resistance). The high-frequency intercept of the impedance spectra corresponds to the specific ohmic resistance of the symmetric cell (R_Ω), including the ohmic resistance of the ScSZ electrolyte, ohmic resistance of the cathode, contact resistance at the cathode/electrolyte interface and contact resistance between the cathodes and current collector Pt mesh. R_p is related to the cathodic polarizations associated with oxygen reduction: $O_2 + 4e^- \rightarrow 2O^{2-}$. The results indicated that the specific ohmic resistance (R_Ω) estimated from the high frequency intercepts on real axis of the impedance curves was the largest when the LNF cathode was sintered at 1000 °C. When the

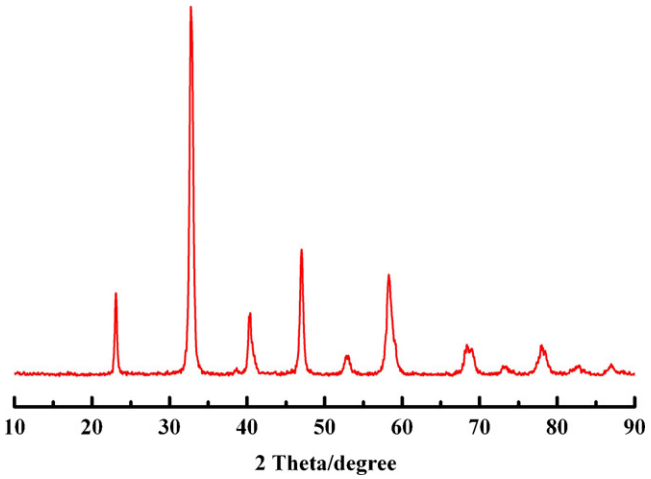

Fig. 2. Powder X-ray diffraction pattern of $LaNi_{0.6}Fe_{0.4}O_{3-\delta}$ powder calcined at 600 °C for 2 h in air.

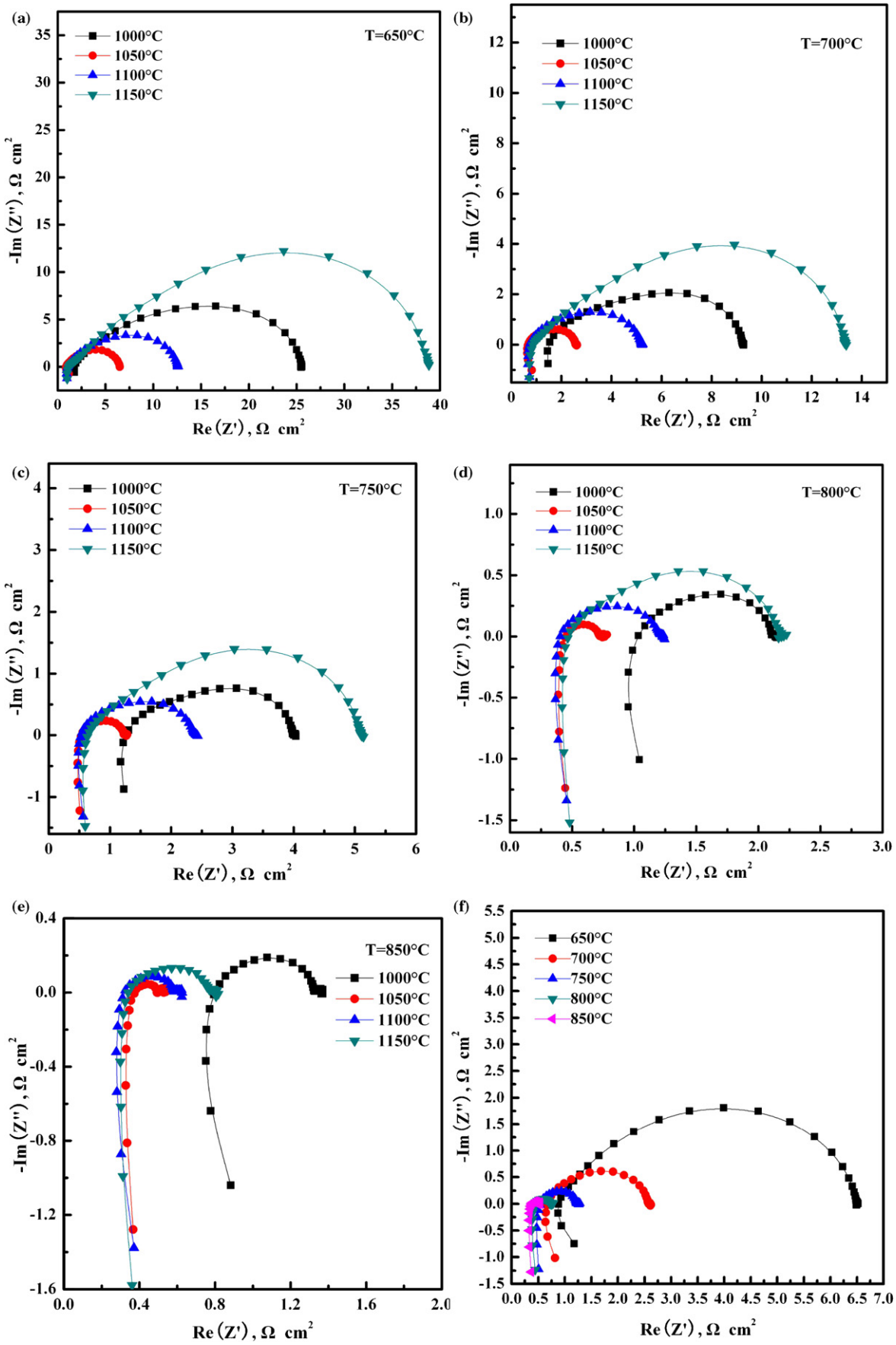

Fig. 3. Electrochemical impedance spectroscopy of the LNF cathode sintered at different temperatures measured at 650 °C (a), 700 °C (b), 750 °C (c), 800 °C (d) and 850 °C (e) in the air, (f) is the impedance spectroscopy of the LNF cathode sintered at 1050 °C measured at different temperatures.

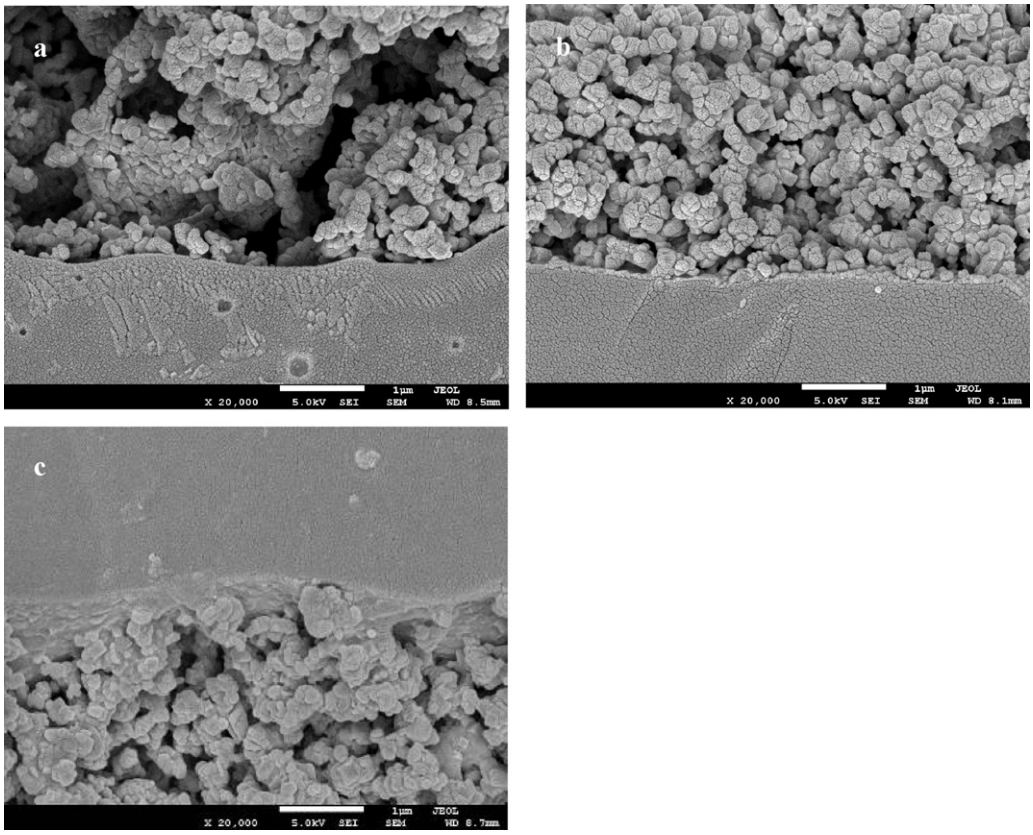

Fig. 4. SEM micrographs of the interface $LaNi_{0.6}Fe_{0.4}O_{3-\delta}$/ScSZ sintered at 1000 °C (a), 1050 °C (b) and 1100 °C (c) for 2 h in the air.

sintering temperature of the LNF cathode increased, R_Ω decreased sharply. The results also indicated that the specific polarization resistance (R_p) estimated from the difference between high and low frequency intercepts on real axis of the impedance curves was the smallest (0.70 Ω cm^2 at 750 °C, 0.27 Ω cm^2 at 800 °C and 0.12 Ω cm^2 at 850 °C) when the LNF cathode was sintered at 1050 °C (shown in Fig. 4(f)). When the sintering temperature of the LNF cathode increased, R_p also increased. It is noted that R_p was the largest when the LNF cathode was sintered at 1150 °C.

Attending to the microstructure, Fig. 4 shows the SEM micrographs of the interface LNF/ScSZ sintered at 1000 °C (a), 1050 °C (b) and 1100 °C (c) for 2 h in the air. The ScSZ electrolyte film is essentially dense, with a continuous and crack free surface morphology and no pinholes. An obvious delamination, which is probably attributed to the lower sintering temperature (1000 °C) of the LNF cathode, is seen in the SEM image of Fig. 4(a). Apparently, this is why the specific ohmic resistance of the symmetric cell with the LNF cathode sintered at 1000 °C was largest. Consequently, the delamination between the LNF cathode layer and the ScSZ electrolyte layer also decreases the triple phase boundaries (TPBs) for the O_2 reduction, R_p is also larger. On the other hand, the microstructure of the LNF cathode sintered at 1050 °C is very promising, a porous structure made of sintered LNF particles (Fig. 4(b)). The SEM images of the interface LNF/ScSZ in Fig. 4(b) show that the LNF cathode layer adheres to the surface of the ScSZ electrolyte layer pretty well without any delamination, which indicates that the LNF cathode layer is thermo-mechanically compatible with the ScSZ electrolyte layer. Results of impedance spectra obtained for the symmetric cell presented in Fig. 3 confirm that the LNF cathode sintered at 1050 °C shows smallest specific polarization resistance. It reveals that a heat-treatment temperature at 1050 °C gives good adhesion between the LNF cathode layer and the ScSZ electrolyte layer, which could enhance the triple phase boundaries for the O_2 reduction, so the value of R_p is the smallest. However, when the sintering temperature was higher than 1050 °C, results of impedance spectra shown in Fig. 3 confirmed that the specific polarization resistance began to increase. The SEM images of the interface in Fig. 4(c) also shows that the LNF cathode layer is well adhered to the ScSZ electrolyte layer. To clarify the phenomenon, we recorded the XRD patterns of the mixture LNF–ScSZ sintered at 1100 °C for 5 h shown in Fig. 5. The formation of insulating $La_2Zr_2O_7$ could be found and became stronger at

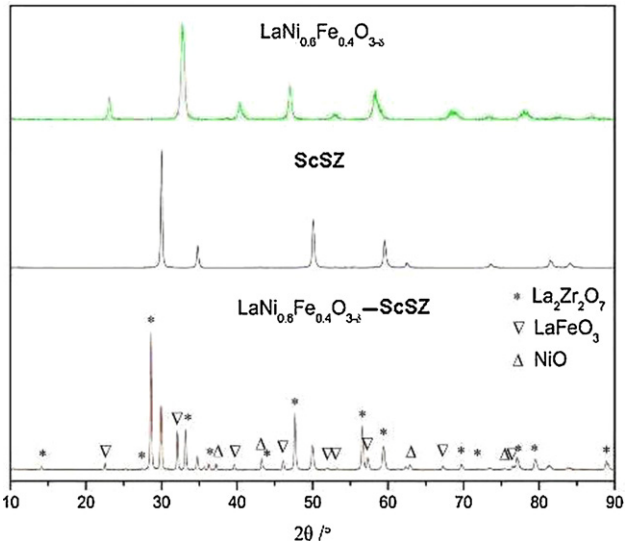

Fig. 5. XRD patterns of $LaNi_{0.6}Fe_{0.4}O_{3-\delta}$, ScSZ and $LaNi_{0.6}Fe_{0.4}O_{3-\delta}$–ScSZ composite powders sintered at 1100 °C for 5 h in the air.

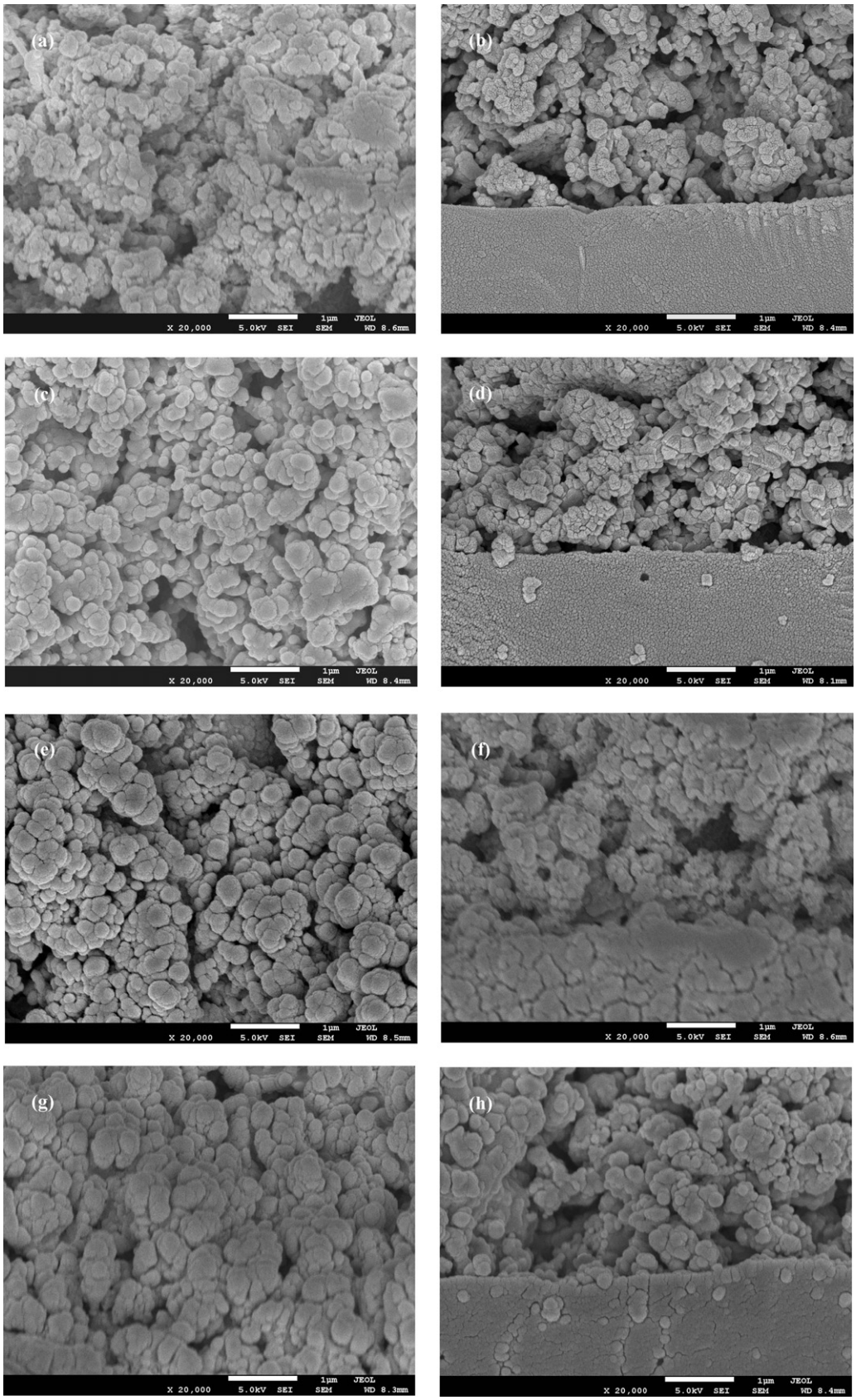

Fig. 6. SEM micrographs of: (a) surface and (b) fractured cross section of pure LNF; (c) surface and (d) fractured cross section of 4.7 wt.% GDC-impregnated LNF; (e) surface and (f) fractured cross section of 8.1 wt.% GDC-impregnated LNF; (g) surface and (h) fractured cross section of 13.9 wt.% GDC-impregnated LNF; (i) and (j) surface and fractured cross section of 15.9 wt.% GDC-impregnated LNF; (k) and (l) surface and fractured cross section of 21.3 wt.% GDC-impregnated LNF; (m) and (n) surface and fractured cross section of 26.9 wt.% GDC-impregnated LNF.

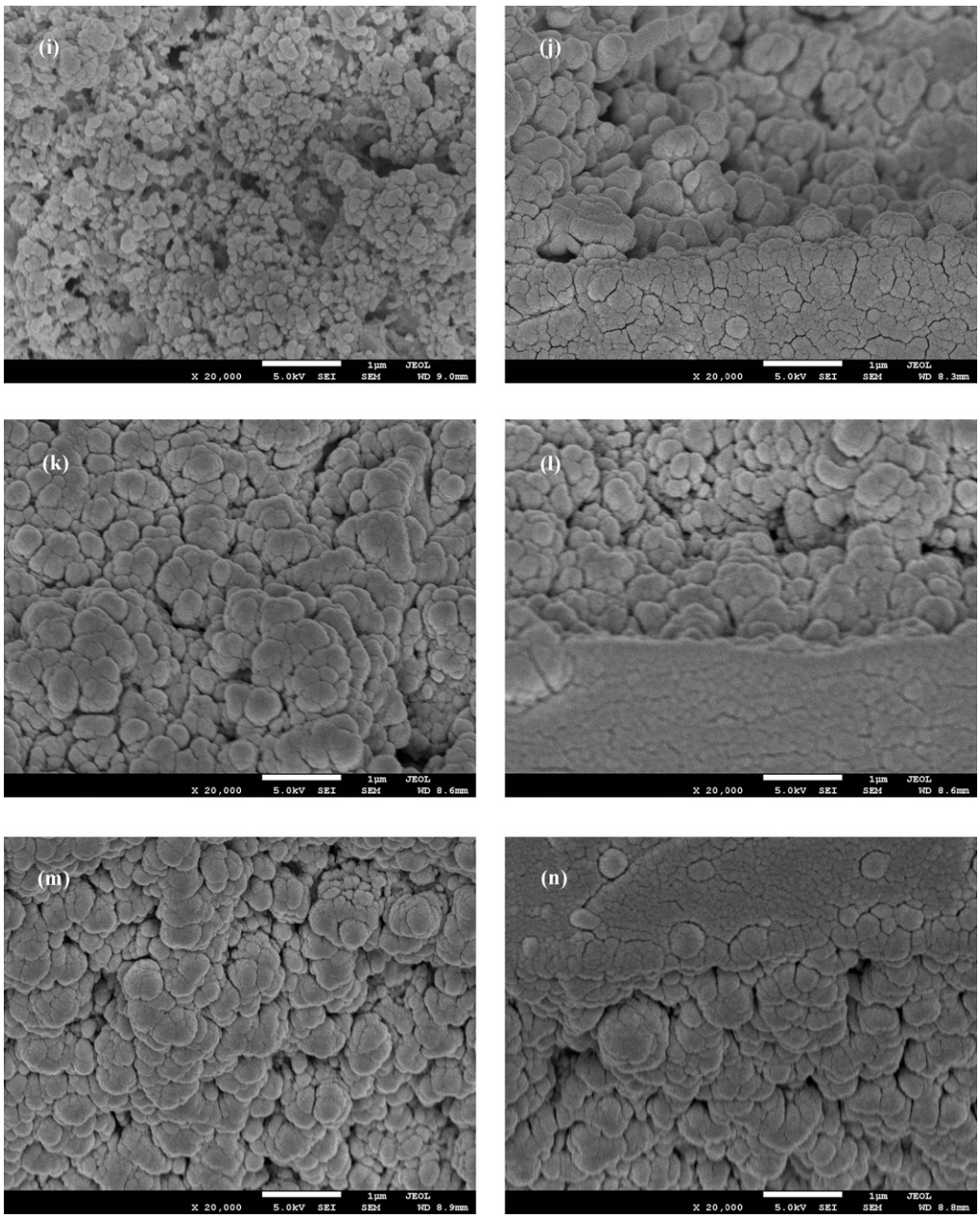

Fig. 6. *(Continued).*

1150 °C. This is why the specific polarization resistance (R_p) was the largest when the LNF cathode was sintered at 1150 °C. Without specification, the LNF cathodes discussed later were sintered at 1050 °C.

The GDC loading of the impregnated LNF cathode was about 4.7 wt.% after one impregnation treatment, and increased to 8.1 wt.%, 13.9 wt.%, 15.9 wt.% and 21.3 wt.% after two, three, four and five times impregnation treatments, respectively. The maximum loading of GDC was 26.9 wt.% after repeating the impregnation processes six times. The porosity of pure LNF cathode was 38.1% and it decreased to 32.2% for the 4.7 wt.% GDC-impregnated LNF cathode. Thus, the volume loading of the impregnated GDC for the 4.7 wt.% GDC-impregnated LNF cathode was 5.9 vol.%. In the case of LNF cathode with the impregnation of 26.9 wt.% GDC, the porosity of the impregnated LNF cathode was almost zero, indicating that volume loading of the GDC was 38.1 vol%. Table 1 shows the GDC loading and porosity of the GDC-impregnated LNF cathodes.

Fig. 6 shows the SEM pictures of the surface and fractured cross section of pure and GDC-impregnated LNF cathodes. Fig. 7 is the EDS patterns of the surface of the 21.3 wt.% GDC-impregnated LNF cathode. Fig. 8 shows the enlarged SEM picture of the fractured cross section of 21.3 wt.% GDC-impregnated LNF cathode. For pure LNF, well-defined and granular-shaped particles with clear grain

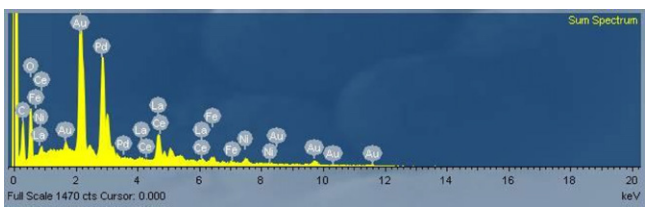

Fig. 7. EDS patterns of the 21.3 wt.% GDC-impregnated LNF cathode.

Table 1
Porosity and GDC loading of the impregnated LNF cathode.

Impregnation cycle	0	1	2	3	4	5	6
Porosity (%)	38.1	32.2	24.6	19.7	13.1	6.2	0.05
Loading in weight (wt.%)	0	4.7	8.1	13.9	15.9	21.3	26.9
Loading in volume (vol%)	0	5.9	13.5	18.4	25.0	31.9	38.1

boundaries were observed (Fig. 6(a) and (b)). The LNF grains were in the range of 0.4–1.0 μm. EDS pattern reveals the presence of the constituent elements of the 21.3 wt.% GDC-impregnated LNF cathode, La, Ni, Fe and Ce (Fig. 7). After the ion impregnation with $Gd_{0.2}Ce_{0.8}(NO_3)_x$ solution, very fine particles were formed around LNF grains (Fig. 6(c) and (d)). The size of impregnated GDC oxide particles was in the range of 40–50 nm, as estimated from the enlarged SEM pictures (Fig. 8). Clearly, the impregnated GDC particles are much smaller than that of LNF particles. The distribution of the nanosized GDC particles appears to be isolated in the case of the 4.7 wt.% GDC-impregnated LNF cathode. With the increase in the GDC loading, there was significant increase in the coverage of the LNF particles by the nanosized GDC particles. This is indicated by the disappearance of the smooth and well-defined morphology of the LNF grains (see Fig. 6(f)). The pores were gradually filled with fine GDC particles and the porosity of the LNF cathodes decreased considerably with the increase in the impregnated GDC loading. In the case of the 26.9 wt.% GDC-impregnated LNF cathode, the pores were almost completely filled by the GDC phase, forming a rather dense structure.

Fig. 9 shows the typical electrochemical impedance spectroscopies of the pure and GDC-impregnated LNF cathodes measured at 650 °C (a), 700 °C (b), 750 °C (c), 800 °C (d) and 850 °C (e) in air. As it can be seen from the corresponding Nyquist plots, the spectra are composed of one semicircle, which is associated with oxygen reduction at the pure or GDC-impregnated LNF/ScSZ interfaces. Fig. 10 shows the effect of the impregnated GDC loading on the specific polarization resistance (R_p) for the O_2 reduction reaction at different temperatures. The R_p of the LNF cathode decreased significantly with the increase in the impregnated GDC loading up to 21.3 wt.%. Further increase in the loading to 26.9 wt.% leads to an increase in the R_p, which may be attributed to the increase in concentration polarization as a consequence of the decreased porosity. For example, the R_p was 0.70 Ω cm^2 for the pure LNF cathode at 750 °C, while it was 0.58 Ω cm^2 for the 4.7 wt.% GDC-impregnated LNF cathode at 750 °C, representing a reduction of 17.14% (Fig. 9(c)) compared to the case of the pure LNF. The R_p reached the lowest value (0.13 Ω cm^2) when 21.3 wt.% GDC is loaded, reduced by 81.43% (Fig. 9(c)) compared with that of the pure LNF cathode at the same temperature. However, in the case of the 26.9 wt.% GDC-impregnated LNF cathode, it was 0.56 Ω cm^2. Similar impedance behavior was also observed for the O_2 reduction reaction on the freshly prepared pure and GDC-impregnated LNF cathodes at other temperatures. In addition, the reduction in the R_p is particularly effective for the GDC-impregnated LNF cathodes at low temperatures (e.g., 650 °C). For the pure LNF cathode, the R_p was 5.59 Ω cm^2 at 650 °C. It was 3.40 and 1.40 Ω cm^2 at 650 °C with the impregnated GDC loading of 4.7 wt.% and 21.3 wt.%, respectively.

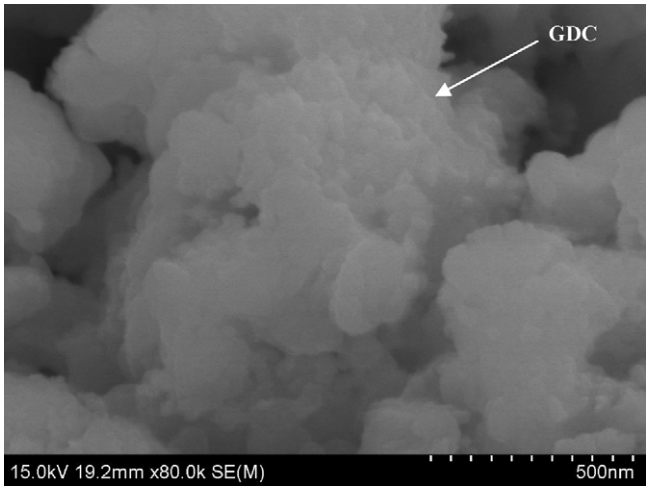

Fig. 8. The enlarged SEM picture of the fractured cross section of 21.3 wt.% GDC-impregnated LNF cathode.

Further investigation indicates that the impregnation of nanosized GDC greatly accelerates the oxygen dissociation and diffusion processes. The enhancement in O_2 reduction kinetics is most likely related to the high electrocatalytic effect and the high surface areas of the impregnated nano-sized GDC phase [24]. The impregnation of the nano-sized ionic conducting GDC phase in the predominantly electronic conducting LNF porous network could substantially enhance the triple phase boundaries for the O_2 reduction. This would be similar to the effect of GDC phase in the LSM/GDC composite cathodes on the promotion of the O_2 reduction reaction rate [29,30]. It is expected that the LNF cathode performance greatly depends on the loading of the impregnated GDC particles since the number of the TPB sites is related to the amount of the impregnated GDC particles, which also greatly affect the LNF cathode microstructures. As an example, Fig. 6 shows the microstructure of the LNF cathodes with different GDC loading. The LNF particles are porous, exhibit irregular shapes with 0.4–1.0 μm in size, and are sintered to form a porous backbone (Fig. 6(b)). At low loading, such as 4.7 wt.% GDC-impregnated LNF cathode, the LNF particles are partially covered with GDC particles, which are at the nanoscale and can be as small as 40 nm (Fig. 8). The distribution of nano-sized GDC particles appears to be isolated on fractured cross section of the backbone (Fig. 6(d)), thus effective TPB is only formed near the cathode/electrolyte physical interface. With the increase of the loading, impregnated particles are gradually connected, forming continuous pathway for oxygen ion conduction, and extending the TPB from the cathode/electrolyte interface to the bulk of the cathode. As an example, when 21.3 wt.% GDC is embedded into the porous backbone, the profile of the exposed LNF backbone disappears, and only a continuous GDC structure formed by the connected GDC particles can be seen (Fig. 8). The microstructure evolution reveals that the advantage of the impregnation method compared to the conventional mechanically mixing method, at least partly, is the presence of fine particles which can generate much more TPBs. Consequently, the specific polarization resistance gradually decreases with the loading. However, obvious aggregation of the GDC particles is observed when 26.9 wt.% GDC is embedded into the porous LNF backbone, and pores are almost filled with the GDC particles (Fig. 6(m) and (n)), which leads to the increase of R_p resulting from the decrease in the active surface as a consequence of the decreased porosity in dense LNF/GDC cathode.

Fig. 11 compares the specific polarization resistance (R_p) of the GDC-impregnated LNF cathodes in this study with those of the pure LSM, LSM/YSZ, LSM/GDC, and the mixed ionic and electronic conducting (La,Sr)(Co,Fe)O_3 (MIEC) cathodes reported in the

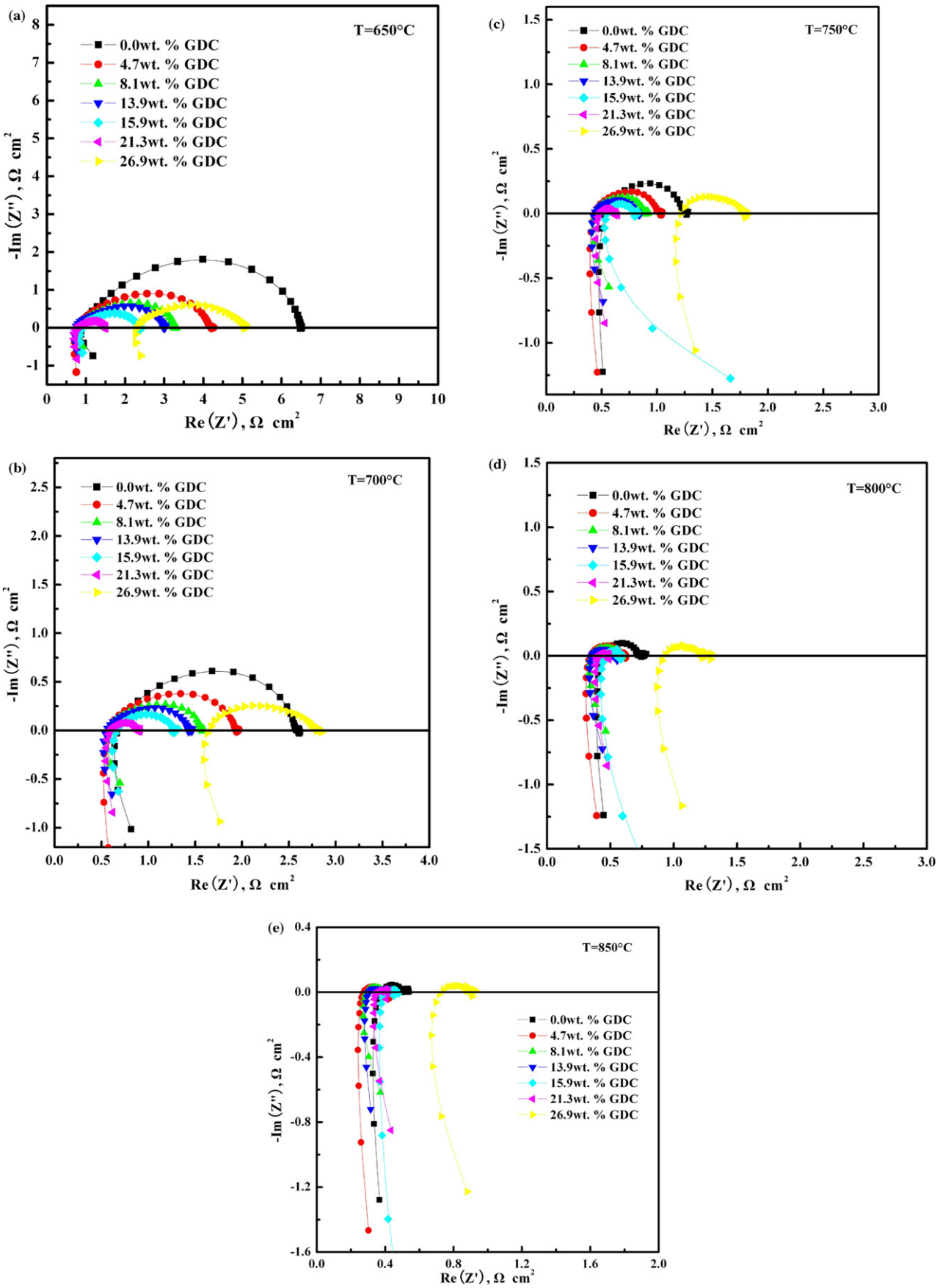

Fig. 9. Electrochemical impedance spectra of the freshly prepared LNF cathodes with and without the GDC-impregnation treatment measured at 650 °C (a), 700 °C (b), 750 °C (c), 800 °C (d) and 850 °C (e) in air. EIS was measured at open circuit.

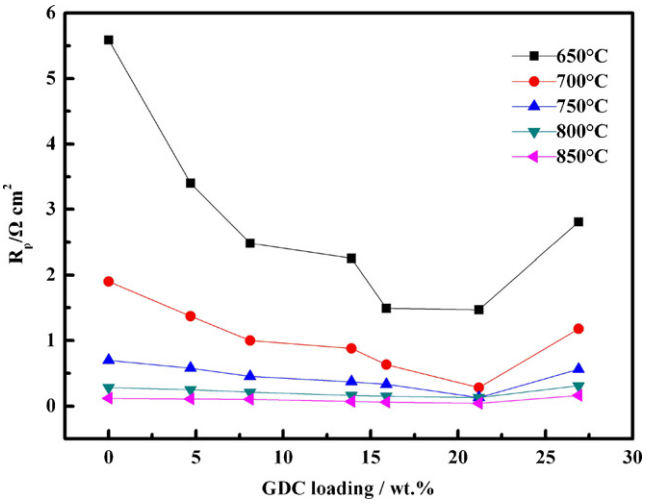

Fig. 10. Dependence of R_p of GDC-impregnated LNF cathodes on the GDC loading. The R_p values were measured at different temperatures.

literature. For the O_2 reduction reaction on the pure LNF cathode, R_p varied slightly from 0.7 to 0.75 Ω cm^2 and from 1.9 to 2.4 Ω cm^2 at 750 °C and 700 °C, respectively [31]. With the addition of 30 wt.% CGO phase in the LNF cathode, R_p of the LNF/CGO composite cathode was reduced to 0.28 Ω cm^2 and 0.61 Ω cm^2 at 750 °C and 700 °C, respectively [31]. For the O_2 reduction on the 21.3 wt.% GDC-impregnated LNF cathode, R_p was 0.04 Ω cm^2, 0.13 Ω cm^2 and 0.28 Ω cm^2 at 850 °C, 750 °C and 700 °C, respectively, significantly lower than that of LNF/CGO composite cathode. Most significantly, the cathode polarization performance of the 21.3 wt.% GDC-impregnated LNF cathode is comparable to that of LSCF, $La_{0.8}Sr_{0.2}FeO_3$ (LSF) and $Gd_{0.8}Sr_{0.2}CoO_3$ (GSC) cathodes. LSCF is known to be a very good mixed ionic and electronic conductor with high electrocatalytic activity for the O_2 reduction reactions [32]. The R_p for cathodes on GDC electrolyte, displayed in Fig. 11, shows that the cobaltates all achieve performances below 1 Ω cm^2 at 700 °C. The standard $La_{0.6}Sr_{0.4}Co_{0.8}Fe_{0.2}O_3$ and $La_{0.8}Sr_{0.2}Co_{0.8}Fe_{0.2}O_3$ material perform better than most materials,

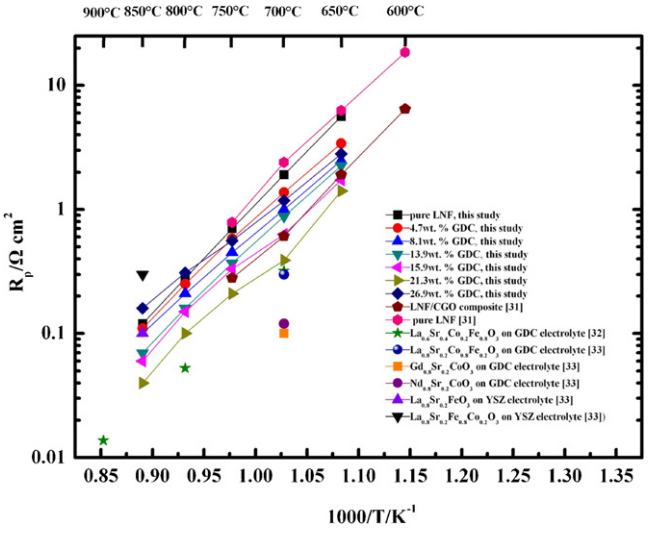

Fig. 11. A comparison of the specific polarization resistance (R_p) of the pure and GDC-impregnated LNF cathodes in this study with that of LNF–CGO composite cathode reported in the literature. Numbers are the references cited and lines are for guides only.

achieving a R_p of 0.31 and 0.3 Ω cm^2 at 700 °C, respectively [32,33]. While $Gd_{0.8}Sr_{0.2}CoO_3$ and $Nd_{0.8}Sr_{0.2}CoO_3$ have much better performances. The R_p of $Gd_{0.8}Sr_{0.2}CoO_3$ cathode on GDC electrolyte is approximately 0.1 Ω cm^2 at 700 °C and displays the lowest activation energy among all the cobaltates measured [33]. The presence of Gd as one of the main constituents in the cathode also reduces the probability of unfavorable reactions with GDC, which itself contains Gd. Thus, $Gd_{0.8}Sr_{0.2}CoO_3$ appears to be a promising new cathode material for use with GDC. Clearly, as far as the R_p for cathodes on YSZ electrolyte is concerned, the cathode compositions with the greatest performance are $La_{0.8}Sr_{0.2}FeO_3$ (LSF) and $La_{0.8}Sr_{0.2}Fe_{0.8}Co_{0.2}O_3$ (LSFC), which reach R_p close to 0.1 Ω cm^2 and 0.3 Ω cm^2 at 850 °C, respectively. However, the 21.3 wt.% GDC-impregnated LNF cathode reported in this study shows compatible performance with those of the MIEC conducting cathodes.

4. Conclusions

The nano-structured cathode prepared by the impregnation method has been demonstrated to be very promising for high-performance intermediate-temperature solid oxide fuel cells. The fabrication and performance of GDC-impregnated LNF cathodes were investigated. The microstructure of the GDC-impregnated LNF cathode was characterized by the continuous and porous LNF network with the deposition of nanosized GDC particles. High electrochemical activity has been achieved for the O_2 reduction on the GDC-impregnated LNF cathodes. For example, in the case of the 21.3 wt.% GDC-impregnated LNF cathode, extremely low specific polarization resistance of the cathode of 0.13 Ω cm^2 at 750 °C was obtained.

Acknowledgements

The authors thank the National High Technology Research and Development “863” Program of China (No. 2009AA034400) and the Specialized Research Fund for the Doctoral Program of Higher Education of Ministry of Education (No. 20100073120055) for the grants that support this research.

References

[1] B.C.H. Steele, A. Heinzel, Nature 414 (2001) 345.
[2] T. Ishihara, J. Tabuchi, S. Ishikawa, J. Yan, M. Enoki, H. Matsumoto, Solid State Ionics 177 (2006) 1949.
[3] R. Polini, A. Falsetti, E. Traversa, O. Schaf, P. Knauth, J. Eur. Ceram. Soc. 27 (2007) 4291.
[4] R. Polini, A. Pamio, E. Traversa, J. Eur. Ceram. Soc. 24 (2004) 1365.
[5] Y.J. Leng, S.H. Chan, S.P. Jiang, K.A. Khor, Solid State Ionics 170 (2004) 9.
[6] R. Chiba, F. Yoshimura, Y. Sakurai, Solid State Ionics 124 (1999) 281.
[7] R. Chiba, F. Yoshimura, Y. Sakurai, Solid State Ionics 152 (2002) 575.
[8] H. Orui, K. Watanabe, R. Chiba, M. Arakawa, J. Electrochem. Soc. 151 (9) (2004) A1412.
[9] S. Li, J. Sun, X. Sun, B. Zhu, Electrochem. Solid State Lett. 9 (2006) A86.
[10] A. Weber, R. Manner, E. Ivers-Tiffee, Denki Kagaku 64 (1996) 582.
[11] E. Ivers-Tiffée, A. Webe, K. Schmid, V. Krebs, Solid State Ionics 174 (2004) 223.
[12] N.Q. Minh, J. Am. Ceram. Soc. 76 (1993) 563.
[13] J. Knudsen, P.B. Friehling, N. Bonanos, Solid State Ionics 176 (2005) 1563.
[14] R. Chiba, Y. Tabata, T. Komatsu, H. Orui, K. Nozawa, M. Arakawa, H. Arai, Solid State Ionics 178 (2008) 1701.
[15] C. Xia, Y. Zhang, M. Liu, Electrochem. Solid State Lett. 6 (2003) A290.
[16] C.R. Xia, W. Rauch, W. Wellborn, M. Liu, Electrochem. Solid State Lett. 5 (2002) A217.
[17] Y. Liu, S. Zha, M. Liu, Adv. Mater. (Weinheim Ger.) 16 (2004) 256.
[18] Y. Liu, C. Compson, M. Liu, J. Power Sources 138 (2004) 194.
[19] H. Mitsuyasu, Y. Nonaka, K. Eguchi, Solid State Ionics 113–115 (1998) 279.
[20] Y. Xiong, K. Yamaji, N. Sakai, H. Kishimoto, T. Horita, M.E. Brito, H. Yokokawa, J. Electrochem. Soc. 153 (12) (2006) A2198.
[21] W. Zhu, D. Ding, C. Xia, Electrochem. Solid State Lett. 11 (2008) B83.
[22] S.P. Jiang, Y.J. Leng, S.H. Chan, K.A. Khor, Electrochem. Solid State Lett. 6 (2003) A67.
[23] S.P. Jiang, W. Wang, Solid State Ionics 176 (2005) 1351.
[24] S.P. Jiang, W. Wang, J. Electrochem. Soc. 152 (7) (2005) A1398.

[25] Y. Larring, T. Norby, J. Electrochem. Soc. 147 (2000) 3251.
[26] S. Jain, K. Adiga, V. Vrneker, Combust. Flame 40 (1981) 71.
[27] Z.P. Shao, S.M. Haile, Nature 431 (2004) 170.
[28] S.P. Jiang, J. Mater. Sci. 38 (2003) 3775.
[29] E.P. Murray, S.A. Barnett, Solid State Ionics 143 (2001) 265.
[30] Y.N. Kim, A. Manthiram, J. Electrochem. Soc. 158 (10) (2011) B1206.
[31] J.Y. Chen, S.R. Wang, T.L. Wen, J.L. Li, J. Alloys Compd. 487 (2009) 377.
[32] S.P. Jiang, Solid State Ionics 146 (2002) 1.
[33] J.M. Ralph, A.C. Schoeler, M. Krumpelt, J. Mater. Sci. 36 (2001) 1161.